Journal of Quantitative Spectroscopy & Radiative Transfer 257 (2020) 107362

Contents lists available at ScienceDirect

Journal of Quantitative Spectroscopy & Radiative Transfer

journal homepage: www.elsevier.com/locate/jqsrt

The Angstrom exponents of black carbon aerosols with non-absorptive coating: A numerical investigation

Xiaolin Zhang[a,b,c,d,*], Mao Mao[a,c,*], Hongbin Chen[b], Shihao Tang[d]

[a] *Key Laboratory of Meteorological Disaster, Ministry of Education (KLME) / Earth System Modeling Center (ESMC) / Collaborative Innovation Center on Forecast and Evaluation of Meteorological Disasters (CIC-FEMD) / Joint International Research Laboratory of Climate and Environment Change (ILCEC) / Key Laboratory for Aerosol-Cloud-Precipitation of China Meteorological Administration, Nanjing University of Information Science & Technology, Nanjing 210044, China*

[b] *Key Laboratory of Middle Atmosphere and Global Environment Observation (LAGEO), Institute of Atmospheric Physics, Chinese Academy of Sciences, Beijing 100029, China*

[c] *School of Atmospheric Physics, Nanjing University of Information Science & Technology, Nanjing 210044, China*

[d] *National Satellite Meteorological Center, China Meteorological Administration, Beijing 100081, China*

ARTICLE INFO

Article history:
Received 5 August 2020
Revised 2 September 2020
Accepted 30 September 2020
Available online 1 October 2020

Keywords:
Black carbon aerosol
Angstrom exponent
Coating
Numerical investigation
Single scattering albedo Angstrom exponent

ABSTRACT

Black carbon (BC) aerosols exert important effects on regional and global climate, whilst there still are significant uncertainties in their optical properties, particularly the spectral varying Angstrom exponents. This study numerically evaluates the influences of coating morphologies on optical properties of BC with non-absorbing coating, and evaluates the sensitivity of their Angstrom exponents, including extinction Angstrom exponent (EAE), absorption Angstrom exponent (AAE) and single scattering albedo Angstrom exponent (SSAAE), to particle microphysics with the multiple-sphere T-matrix method. Among all microphysical parameters, the shell/core ratio and size distribution play substantial roles in determining the EAE, AAE and SSAAE of coated BC, wherein the dependences of the Angstrom exponents on size distribution are higher. The EAE, AAE and SSAAE of coated BC by non-absorptive materials with different particle size distributions change in ranges of 0.3–1.5, 0.3–2.5 and −0.1–0.9, respectively. The core-shell Mie model can hardly produce accurate results of the Angstrom exponents of coated BC particles, especially the AAE and SSAAE. Our study reveals that BC coated by non-absorbing materials with large size distribution of coated BC may show negative SSAAE values for some coating microphysics, indicating the limitation of separating brown carbon from black carbon with a criterion of negative SSAAE.

1. Introduction

Aerosols, released from anthropogenic and natural sources, are widespread in ambient air and show significant effects on regional and global climate, as well as the environment [e.g., 1]. As one of the strongly absorptive aerosols, black carbon (BC) contributes significant positive radiative forcing, being regarded as an important contributor to global warming after carbon dioxide [e.g., 2]. Furthermore, BC can be coated by secondary aerosol species due to aging process, forming complex internal-mixed particles, and resulting in complicated microphysical, optical and radiative properties [3]. Lacking precise understanding and appropriate parameterization of wavelength-dependent optical and radiative properties of aged BC particles has been an important limitation in the accurate assessment of their radiative forcing [4,5].

Optical and radiative properties of aged BC are substantially impacted by its microphysical properties [e.g., 6], whereas more and more aged BC microphysics have been revealed based on recent observations. The aged BC observations from biomass burning quantify that almost half BC particles are fully encapsulated and about one third are partially coated [7]. Dominated fully and partially coated BC morphologies are also seen for BC aerosols at a marine site of Portugal, which can receive air pollutions from several continents through long-range transports [8]. The measurements by single-particle soot photometer show that shell/core ratio D_p/D_c (particle diameter divided by BC core diameter) can vary between 1.1 and 2.1 in London [9], whereas a range of 2.1–2.7 is seen in Beijing [10]. These observed coated BC microphysical properties are the basis for a better simulation of their optical and radiative properties based on numerical modeling. Fractal aggregates have been widely accepted as BC numerical geometry to simulate

* Corresponding authors.
E-mail addresses: xlnzhang@nuist.edu.cn (X. Zhang), mmao@nuist.edu.cn (M. Mao).

https://doi.org/10.1016/j.jqsrt.2020.107362
0022-4073/

BC optical and radiative properties, as they show good similarity to realistic BC geometries [e.g., 11]. Meanwhile, BC aggregates with dispersal monomers or overlapping are considered [e.g., 12], whereas complicated models of coated BC are also built for coating effects [e.g., 2,13]. Furthermore, the core-shell Mie model is a popular model extensively applied in remote sensing and radiative transfer due to high efficiency and simplicity, whilst its performance in approximating optical properties of coated BC, particularly the spectral varying properties, is still an open question [e.g., 13].

Among optical properties of aerosols, Angstrom exponents are significant properties that are used to express relative intensities of extinction, absorption or single scattering albedo at different incident wavelengths and to infer aerosol information, such as type and size. The extinction Angstrom exponent (EAE), absorption Angstrom exponent (AAE) or single scattering albedo Angstrom exponent (SSAAE) indicate the wavelength dependences of aerosol extinction, absorption, or single scattering albedo, respectively [14]. The EAE is regarded to be in association with particle size, whereas it is not strictly indicative of size due to its dependence on aerosol absorption [e.g., 15]. The values of EAE less than 1 and larger than 1 implies that particles are dominated in coarse and fine modes, respectively [e.g., 16]. The AAE gives information of aerosol absorbing types, describing wavelength variation of particle absorption [e.g., 17]. For example, the AAE around 1.0 indicates that particles are pure BC, while BC coated by non-absorbing materials can show an AAE of about 1.6 [e.g., 18]. For the SSAAE, Chakrabarty et al. [19] present that brown carbon has a negative SSAAE, which can be a criterion for separating brown carbon from black carbon. In addition, the EAE/AAE has also been utilized for studies of estimation of aerosol radiative forcing [e.g., 20]. The Angstrom exponents are significant aerosol optical properties due to containing important particle microphysical information, whilst the research focusing on their theoretical studies is generally limited. Li et al. [21] numerically investigate the Angstrom exponents of bare BC, whereas the Angstrom exponents of aged BC impacted by their microphysics are not known, and this limits the ability to thoroughly understand related measurements in ambient environment and to perform accurate simulations of radiative transfer.

Here, systematic investigations of Angstrom exponents of polydisperse aged BC particles are numerically performed based on current understandings. An accurate multiple-sphere T-matrix method (MSTM) is employed to compute optical properties of coated BC aerosols at several wavelengths and further their Angstrom exponents. This study aims at assessing the impacts of coated BC microphysics, including size distribution, coated volume fraction of BC, BC geometry, BC position inside coating, and shell/core ratio on their Angstrom exponents, which is hopefully beneficial to understanding and application of aerosol Angstrom exponents.

2. Methodology: BC models and numerical simulation

The observations show that freshly emitted BC particles look like cluster-like aggregates with a mass of similar-sized monomers [e.g., 2], and their geometries can be successfully described with the fractal aggregates, mathematically following:

$$N = k_0\left(\frac{R_g}{a}\right)^{D_f}, \tag{1}$$

$$R_g = \sqrt{\frac{1}{N}\sum_{i=1}^{N} r_i^2}, \tag{2}$$

where D_f, N, k_0, a and R_g are fractal dimension, monomer number, fractal prefactor, monomer radius, and gyration radius, respectively [e.g., 22]. After emitted, BC ages quickly and can be coated by secondary aerosol species (such as organics) through condensation and coagulation with time going [e.g., 23]. During aging process, BC can collapse and becomes compact with a D_f near 3, whereas fresh BC particles generally exhibit small D_f with values less than 2 [24,25]. Based on the observations by China et al. [7,8], aged BC aerosols typically show three coating morphologies, i.e., externally attached, partially coated, and fully encapsulated, and coated volume fraction of BC (F) has been employed to describe these BC coating states [26].

We consider coated BC models developed by Zhang et al. [26], assuming BC aggregates coated by spherical organics with various F values between 0.0 and 1.0, and portraying the sketch maps in Fig. 1 following Zhang et al. [27]. F=0.0, F=1.0, and $0.0 < F < 1.0$ indicate BC aggregates externally attached to, fully encapsulated by, and partially coated by organics, respectively. A tunable particle-aggregation algorithm on the basis of Skorupski et al. [28] is applied to generate BC aggregates. Following Zhang and Mao [6], a N value of 200 is assumed, since ambient BC aerosols are mostly in accumulation mode. A k_0 value of 1.2 is considered [22], and BC D_f values of 1.8 and 2.8 are assumed, signifying loose and compact BC aggregates, respectively [26]. We assume ideal point-contacting monomers for BC aggregates with overlapping and necking neglected, and it should be noticed that overlapping and necking may enhance the single scattering albedo [29]. More detailed descriptions of the model developed can be seen in Zhang et al. [26]. For coated BC, shell/core ratio D_p/D_c within 1.1–2.7 is considered [9,10]. Given that aged BC models are built, a multiple-sphere T-matrix method [30] is employed to exactly compute their optical properties.

For ambient atmospheric applications, optical properties of polydisperse particles averaged over certain size distributions are meaningful, and our study assumes coated BC particles following a lognormal size distribution in form of

$$\mathrm{n}(r) = \frac{1}{\sqrt{2\pi}\,r\ln(\sigma_g)}\exp\left[-\left(\frac{\ln(r)-\ln(r_g)}{\sqrt{2}\ln(\sigma_g)}\right)^2\right], \tag{3}$$

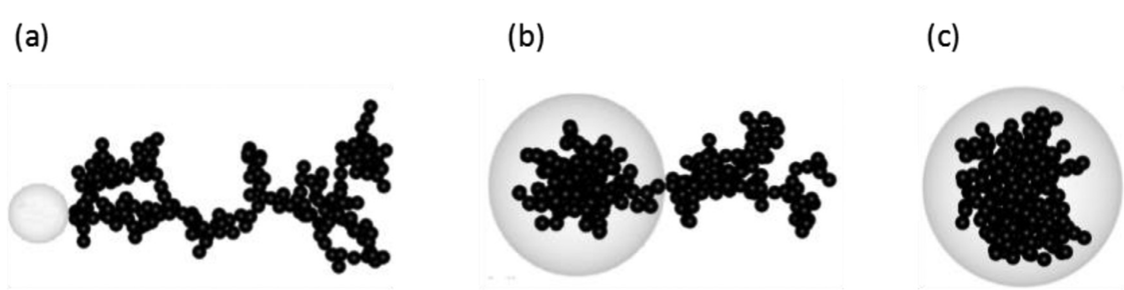

Fig. 1. Sketch maps of geometries of coated black carbon based on Zhang et al. [27]. Examples of fractal black carbon aggregates, containing 200 monomers, are externally attached to (a), partially coated by (b), and fully coated (c) in organics with coated volume fractions of BC being 0.0, 0.5, and 1.0, respectively.

where σ_g denotes geometric standard deviation, and r_g is geometric mean radius [e.g., 31]. We consider r_g and σ_g being 0.075 μm and 1.59, respectively [32], and size range is within 0.1–1 μm, as aged BC is mostly observed in accumulation mode. With size distribution, extinction cross section (C_{ext}), absorption cross section (C_{abs}), and single scattering albedo (SSA) of coated BC can be calculated using

$$\langle C_{ext}\rangle = \int_{r_{\min}}^{r_{\max}} C_{ext}(r)n(r)d(r) \tag{4}$$

$$\langle C_{abs}\rangle = \int_{r_{\min}}^{r_{\max}} C_{abs}(r)n(r)d(r) \tag{5}$$

and

$$\langle SSA\rangle = \frac{\langle C_{ext}\rangle - \langle C_{abs}\rangle}{\langle C_{ext}\rangle}. \tag{6}$$

The EAE, AAE and SSSAE express the dependences of extinction, absorption and single scattering albedo on wavelength, and conventionally, these Angstrom exponents between wavelengths of λ_1 and λ_2 are described with

$$EAE(\lambda_1,\lambda_2) = -\frac{\ln(\langle C_{ext}(\lambda_1)\rangle) - \ln(\langle C_{ext}(\lambda_2)\rangle)}{\ln(\lambda_1) - \ln(\lambda_2)} \tag{7}$$

$$AAE(\lambda_1,\lambda_2) = -\frac{\ln(\langle C_{abs}(\lambda_1)\rangle) - \ln(\langle C_{abs}(\lambda_2)\rangle)}{\ln(\lambda_1) - \ln(\lambda_2)} \tag{8}$$

and

$$SSAAE(\lambda_1,\lambda_2) = -\frac{\ln(\langle SSA(\lambda_1)\rangle) - \ln(\langle SSA(\lambda_2)\rangle)}{\ln(\lambda_1) - \ln(\lambda_2)}. \tag{9}$$

Obviously, the EAE, AAE and SSSAE are negative slopes of extinction, absorption and single scattering albedo of coated BC between wavelengths of λ_1 and λ_2 on log-log scales ($\lambda_2 > \lambda_1$), respectively [e.g., 14]. The Angstrom exponents of coated BC are investigated at wavelengths of 350 nm, 550 nm, and 700 nm in this study, which are similar to the wavelength selections in Luo et al. [33]. BC coatings in the atmosphere may include both absorbing and non-absorbing organics, whereas this study only focuses on BC with non-absorbing coating following Zhang et al. [26]. The refractive indices of non-absorbing organics and BC are assumed to be wavelength-independent, being $1.55 - 0i$ [19], and $1.85 - 0.71i$ [34] for three wavelengths considered, respectively. It should be noted that BC refractive indices have large uncertainties with an upper-bound of $1.95 - 0.79i$ and a lower-bound of $1.75 - 0.63i$ [34], while the real part of refractive index of non-absorbing organics can vary between 1.35 and 1.61 due to chemical and physical complexities [19,35]. Zhang et al. show that absorption enhancement of BC due to non-absorptive coating has low sensitivity to BC refractive index [36].

3. Results and discussion

3.1. Optical properties of coated BC at a single wavelength

Optical properties of coated BC with a shell/core ratio of 1.9 for different geometries at an incident wavelength of 550 nm are compared in Table 1. We consider two fractal dimensions of BC with D_f of 1.8 and 2.8, and five coated volume fractions of BC with F from 0.0 to 1.0, as well as the popular core-shell Mie model. The optical properties are averaged for an ensemble of coated BC with the aforementioned size distribution. For a fixed F, the C_{ext} of coated BC increases as BC D_f increases from 1.8 to 2.8, indicating that compact coated BC shows larger C_{ext} than loose one, which is consistent with the results of bare BC presented in Li et al. [21]. With increased F, the sensitivity of the C_{ext} of coated BC to BC D_f becomes decreasing, i.e., showing decreased difference. The influence of BC position inside coating on the C_{ext} is negligible with difference less than 1%, although the C_{ext} of coated BC with BC aggregates at an outmost position within coating is slightly higher than that with BC at particle geometric center. The C_{ext} of equivalent-volume core-shell Mie model is close to that of coated BC aggregates with high F, whereas it can be over 10% higher than that of coated BC aggregates with low F. The impact of BC D_f on the C_{abs} of coated BC is trivial with differences less than 1%, whereas with F increasing from 0.0 to 1.0, the C_{abs} of coated BC aggregates increases by a factor of ~2. This may be associated with the lensing effect of BC due to coating, which is affected by F [26]. The lensing effect is that non-absorbing coatings on BC can enhance BC absorption, and scattering material can focus more photons onto BC core [37], while the sunglasses effect may also be an influence factor for the absorption of coated BC [33]. Zhang et al. also find that BC D_f has negligible influence on the C_{abs} of BC fully coated with non-absorbing coating [36]. The C_{abs} given by the volume equivalent core-shell Mie model is significantly larger than that of coated BC aggregates, and the core-shell Mie model overestimates more for smaller F. Even for fully coated structure, the core-shell Mie model gives larger C_{abs} than that of coated BC aggregates by about 15%. Given the absorption and extinction, it is expected that coated BC SSA decreases with more BC aggregates coated by organics, and the core-shell Mie model underestimates the SSA by at least 10%. Briefly, three important conclusions may be obtained from Table 1. Firstly, in spite that the fractal dimension of BC has significant influences on optical properties of bare BC aggregates [21], its impacts on optical properties of BC with non-absorptive coating are negligible. Secondly, the coated volume fraction of BC, as a microphysical parameter characterizing BC coating state, shows important effects on optical properties of coated BC, particularly for its absorption, which can vary by a factor of ~2, highlighting the importance of coated volume fraction of BC in ambient measurements. Thirdly, the core-shell Mie model can produce acceptable optical properties of coated BC for high coated volume fraction of BC (i.e., near 1.0), whereas significant errors may be introduced for low coated volume fraction of BC, especially for the absorption.

To exhibit clearer comparisons of optical properties of coated BC with various coating morphologies, Fig. 2 shows the results as a function of shell/core ratio at all three wavelengths for coated BC with the aforementioned particle size distribution. With increasing D_p/D_c, the C_{ext} and C_{abs} of coated BC aggregates decrease, as opposed to an increase of SSA. The C_{ext}, C_{abs} and SSA of coated BC aggregates become less sensitive to F, as D_p/D_c becomes larger. The optical properties of equivalent-volume core-shell Mie model under some BC microphysics significantly differ from those of coated BC aggregates with small coated volume fraction of BC. However, the core-shell Mie model can generally approximate optical properties of coated BC aggregates with high coated volume fraction of BC. The C_{ext}, C_{abs} and SSA of coated BC aggregates with the aforementioned fixed size distribution decrease with increased wavelength, indicating positive EAE, AAE and SSAAE, which will be investigated in the following subsection.

3.2. The Angstrom exponents of coated BC

3.2.1. The EAE of coated BC

Fig. 3 illustrates the EAE, AAE and SSAAE values of coated BC with the aforementioned particle size distribution. Two results of Angstrom exponents are discussed: values of subscribe “1” (for example, EAE_1, AAE_1 and $SSAAE_1$) correspond to results on the basis of extinctions, absorptions and SSAs of coated BC at wavelengths of 350 nm and 550 nm, while “2” refers to values between 550 nm and 700 nm. As illustrated in Fig. 3a–f, the EAE of coated BC aggregates is sensitive to D_p/D_c and F, and it increases with increased D_p/D_c or decreased F. Starting from BC D_f of 2.8, with an increase

Table 1
Extinction cross section (C_{ext}), absorption cross section (C_{abs}), single scattering albedo (SSA), and asymmetry factor (g) of coated BC aggregates with shell/core ratio D_p/D_c of 1.9 at a wavelength of 550 nm.

Geometry		C_{ext} ($\times 10^{-2}$ μm^2)	C_{abs} ($\times 10^{-2}$ μm^2)	SSA
$F = 0.00$	D_f =1.8	7.18	1.55	0.78
	D_f =2.8	7.41	1.53	0.79
$F = 0.25$	D_f =1.8	7.52	1.88	0.75
	D_f =2.8	7.67	1.83	0.76
$F = 0.50$	D_f =2.8	7.89	2.22	0.72
$F = 0.75$	D_f =2.8	8.10	2.60	0.69
$F = 1.00$	D_f =2.8 center[a]	8.39	3.09	0.63
	D_f =2.8 outer[b]	8.41	3.01	0.64
Equivalent concentric sphere		8.32	3.55	0.57

[a] BC aggregates at the geometric center of coating.
[b] BC aggregates at an outmost position inside coating.

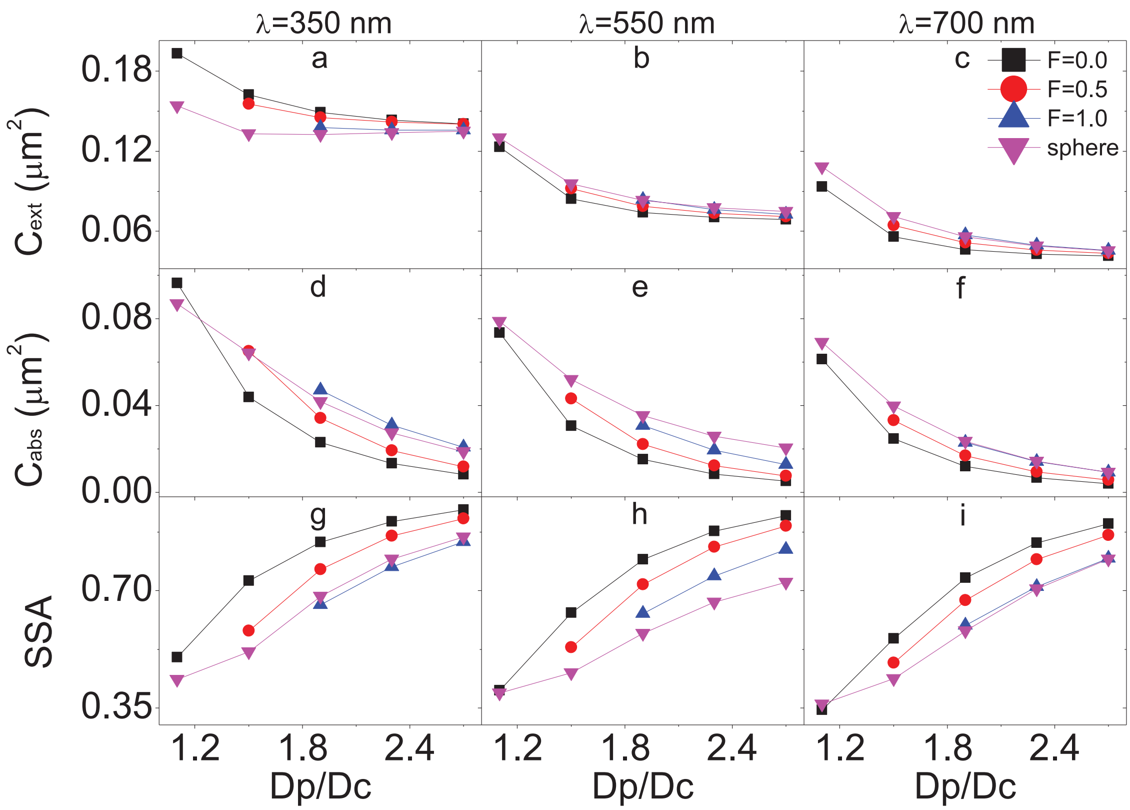

Fig. 2. Extinction cross section (C_{ext}), absorption cross section (C_{abs}), single scattering albedo (SSA), and asymmetry factor (g) of coated BC as a function of shell/core ratio (Dp/Dc) at 350 nm (left), 550 nm (middle), and 700 nm (right). Black squares, red circles, and blue up-triangles indicate coated volume fractions of BC (F) of 0.00, 0.5, and 1.00, respectively, while magenta down-triangles denote relevant results of core-shell Mie model. BC D_f of 2.8 is considered, whereas for $F = 1.0$, BC aggregates is located at particle geometric center.

of D_p/D_c from 1.1 to 2.7, the EAE_1 values of coated BC aggregates with F=0.0 increase from 1.0 to 1.6, while their EAE_2 values vary between 1.1 and 2.1. With F being a moderate value of 0.5, the EAE_1 and EAE_2 of coated BC change in ranges of 1.2–1.5 and 1.5–2.0, respectively, as D_p/D_c increases from 1.5 to 2.7. For fully coated BC with F=1.0, BC positions inside coating result in the EAE differences within 3%, and the EAE_1 and EAE_2 of coated BC aggregates with D_p/D_c from 1.9 to 2.7, are in ranges of 1.1–1.4 and 1.6–2.0, respectively. The EAE values of coated BC aggregates are also sensitive to BC D_f, showing relatively low values for compact coated BC, and the sensitivities become weaker as D_p/D_c or F become larger. The differences of the EAE values induced by BC D_f are negligible, except for thinly coated BC with F=0.0. The EAE of coated BC aggregates is sensitive to wavelength selection, and it becomes more sensitive to coating morphology with the wavelength becoming larger. This is a valuable addition to the previous numerical study of bare BC results presented by Li et al. [21]. For fixed size distribution, the EAE_1 given by the core-shell Mie model is smaller than that of coated BC aggregates, whilst the core-shell Mie model only produces close EAE_2 results to those of thickly coated BC aggregates.

Fig. 4 shows the EAE variations of coated BC at different size distributions, and three structures of coated BC (BC D_f of 2.8) with F=0.0, 0.5 and 1.0, and the core-shell Mie model are considered. The lognormal particle size distributions with r_g ranging from 0.05 μm to 0.15 μm, and σ_g of 1.59 are assumed for coated BC aerosols. Fig. 4 clearly illustrates that the EAE of coated BC is sensitive to both size distribution and shell/core ratio, and the sensitivity of the EAE to size distribution is higher than shell/core ratio. The EAE values of coated BC decrease as r_g increase, i.e., particles becoming larger. For coated BC with F=0.0, the EAE_1 shows wide variation for various size distributions with a range of 0.4–

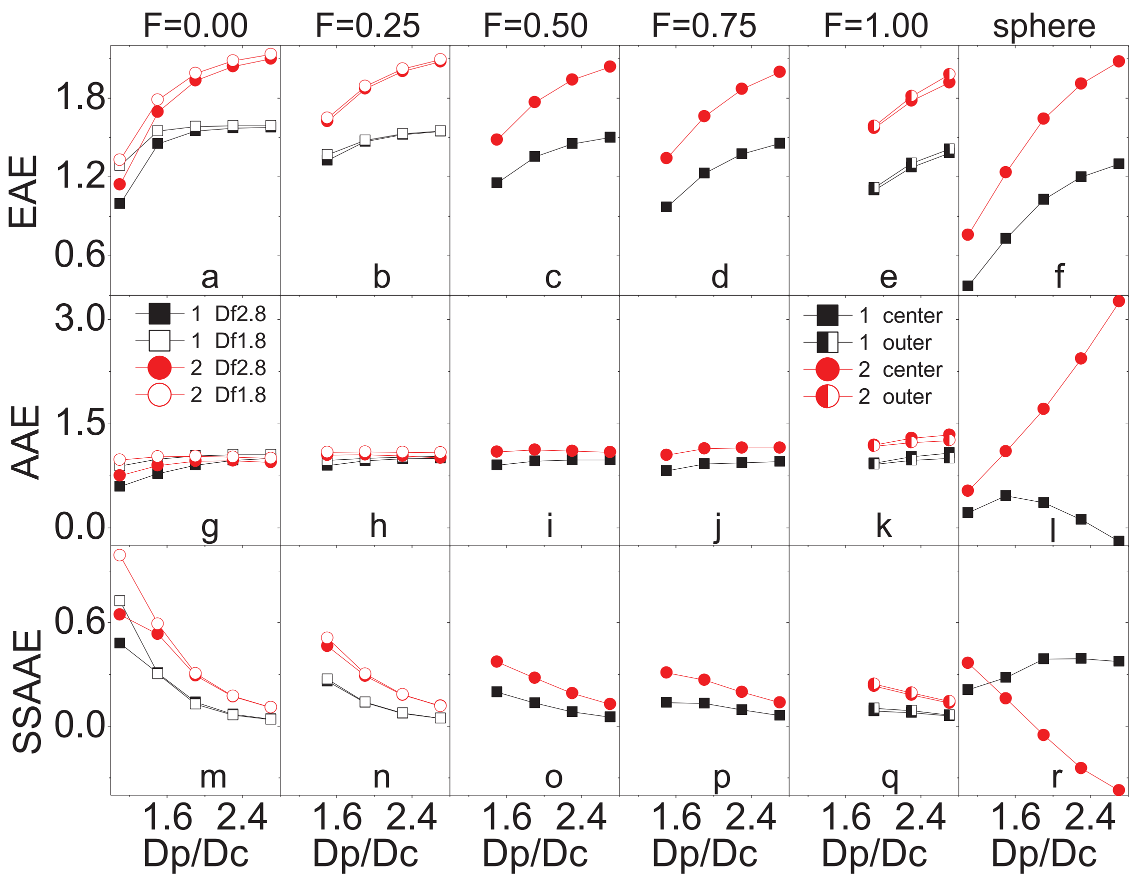

Fig. 3. Angstrom exponents of coated BC as a function of shell/core ratio (Dp/Dc). Extinction Angstrom exponent (EAE, upper row), absorption Angstrom exponent (AAE, middle row), and single scattering albedo Angstrom exponent (SSAAE, bottom row) are considered. Results of coated volume fractions of BC (F) of 0.00, 0.25, 0.50, 0.75, and 1.00, as well as core-shell Mie model are shown from left to right. Black squares and red circles indicate Angstrom exponents of coated BC between 350 nm and 550 nm, and between 550 nm and 700 nm, respectively. Solid and open symbols denote D_f values of BC aggregates being 2.8 and 1.8, respectively. For $F = 1.0$, solid symbols indicate BC aggregates at particle geometric center, whereas half-solid symbols imply BC at an outmost position close to coating boundary.

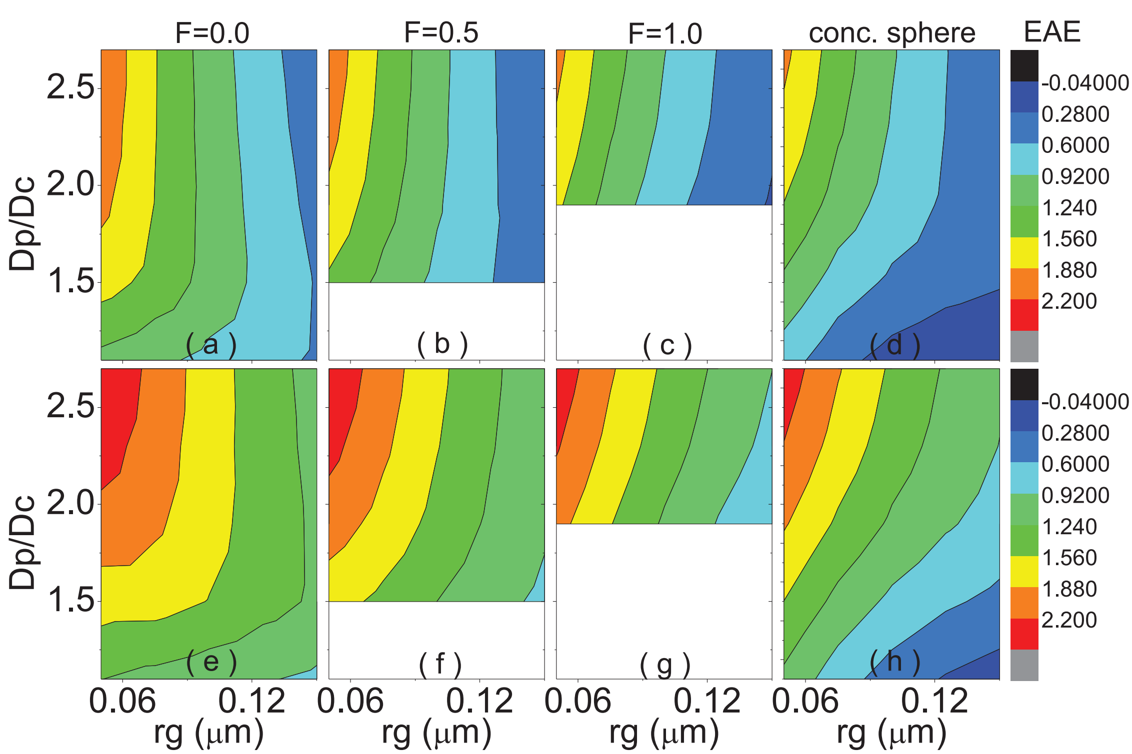

Fig. 4. Extinction Angstrom exponent (EAE) of coated BC aggregates (BC fractal dimension of 2.8) with different shell/core ratio (D_p/D_c) and particle size distribution. The EAEs between 350 nm and 550 nm (upper row), and between 550 nm and 700 nm (bottom row) are considered. Results of coated volume fractions of BC (F) of 0.00, 0.50, and 1.00, as well as core-shell Mie model are shown from left to right. For fully coated BC structure, BC is located at the particle geometric center. The geometric standard deviations (σ_g) for applied lognormal distribution are 1.59.

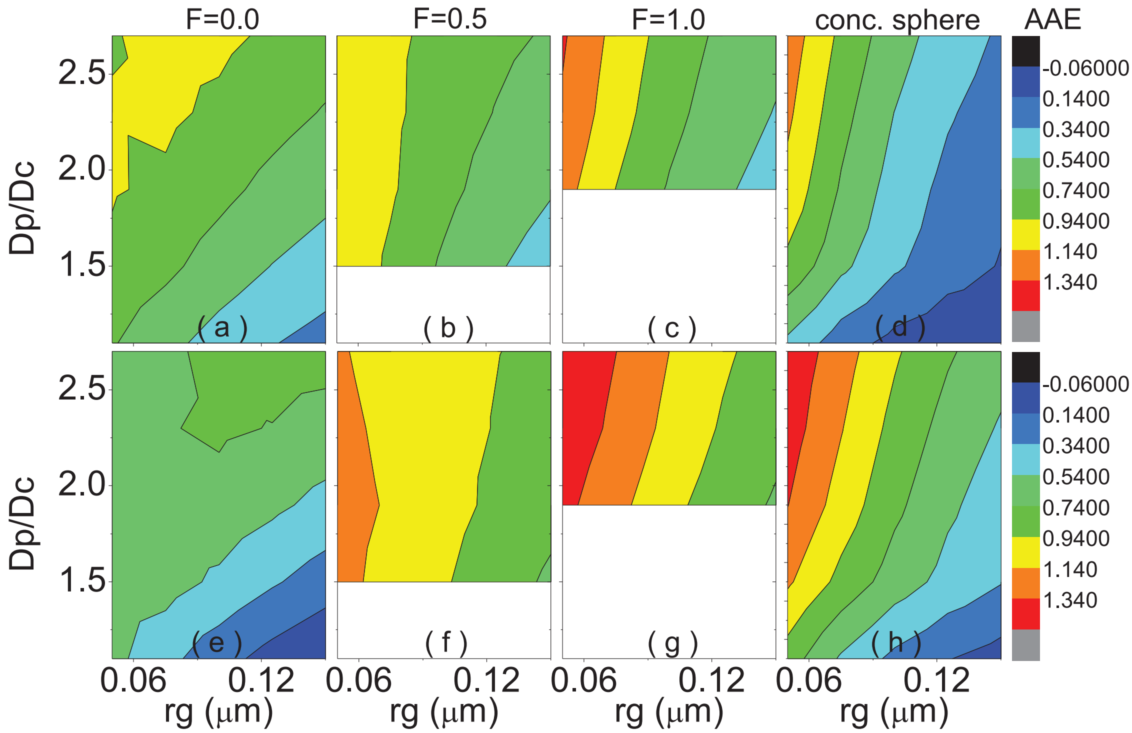

Fig. 5. Same as in Fig. 4 but for AAE.

2.1. Nevertheless, as F is increased to 1.0, the EAE_1 of coated BC becomes slightly low, and its values change from 0.3 to 2.0. The EAE_2 exhibits similar pattern to that of the EAE_1, and its values are higher than those of the EAE_1 of coated BC with the same microphysics, which vary in ranges of 0.9–2.5 and 0.7–2.4 for F of 0.0 and 1.0, respectively. The EAE given by the core-shell Mie model can even show negative values for coated BC with thin coating, and only shows close values to those of coated BC aggregates with some coating microphysics. The EAE value is commonly an indicator for predominant particle size [e.g., 38], and it can be employed to distinguish the fine and coarse aerosols [e.g., 39]. However, caution should be taken in the interpretation of the EAE as an absolute reference to distinguishing particle size, as the EAE is also significantly dependent on shell/core ratio, especially for thinly coated BC.

3.2.2. The AAE of coated BC

The AAE results of coated BC with the aforementioned fixed particle size distribution are shown in Fig. 3g–l. Obviously, the AAE of coated BC aggregates is slightly sensitive to D_p/D_c, F, BC D_f and BC position inside coating, and it becomes less sensitive to BC D_f with increased D_p/D_c or F. For externally attached, partially coated and fully encapsulated BC aggregates, their AAE_1 values are in ranges of 0.6–1.1, 0.8–1.0 and 0.9–1.1, while slightly large AAE_2 with values in ranges of 0.8–1.1, 1.0–1.2 and 1.2–1.3 are seen, respectively. Significant differences between the AAE values of coated BC aggregates with fixed size distribution and those given by the core-shell Mie model are obtained.

Similar to Fig. 4, the results of the AAE_1 and AAE_2 of coated BC with different size distributions are illustrated in Fig. 5. Like the EAE, the AAE of coated BC is highly sensitive to size distribution and shell/core ratio, wherein the sensitivity to size distribution is higher, especially for coated BC with large F. The AAE of coated BC decreases with r_g increasing, and except for the externally attached structure, the AAE_2 is larger than AAE_1 of coated BC with the same coating microphysics. For F=0.0, 0.5 and 1.0, the AAE_1 of coated BC alters in ranges of 0.3–1.0, 0.4–1.1 and 0.5–1.4, respectively, whereas the AAE_2 shows values in ranges of 0.5–1.0, 0.7–1.2 and 0.7–1.5, respectively. The AAE produced by the core-shell Mie model shows wide variation, and is significantly different from that of coated BC aggregates. Liu and Mishchenko also find that the AAE of coated BC is quite sensitive to the choice of wavelength pair, particle morphology and size [40]. Additionally, Liu et al. demonstrate that BC size distribution leads to variations in AAE of bare BC and fully coated BC ranging from 0.8 to over 1.4, and that shape is a significant factor in determining BC AAE [41].

3.2.3. The SSAAE of coated BC

The SSAAE values of coated BC aggregates with the aforementioned fixed size distribution are sensitive to D_p/D_c, and decrease with increasing D_p/D_c, which are portrayed in Fig. 3m–r. The SSAAE of coated BC also shows sensitivity to F, and with increased F, it generally decreases for thin coating, as opposed to an increase for heavy coating. For externally attached structures, the $SSAAE_1$ and $SSAAE_2$ of coated BC with BC D_f of 2.8 are seen in ranges of 0.04–0.48 and 0.11–0.65, respectively, as D_p/D_c varies between 1.1 and 2.7. Meanwhile, for partially coated BC with F=0.5, as D_p/D_c increases from 1.1 to 2.7, the $SSAAE_1$ of coated BC aggregates decreases from 0.20 to 0.05, whereas the $SSAAE_2$ is within 0.13–0.37. While BC aggregates are fully coated, their SSAAE values are almost not sensitive to BC position inside coating with differences less than 5%, and are observed in ranges of 0.06–0.10 and 0.13–0.25 for $SSAAE_1$ and $SSAAE_2$, respectively. The SSAAE of coated BC aggregates is only sensitive to BC D_f for thinly coated structures, and the sensitivity becomes larger as D_p/D_c becomes smaller. In addition, similar to the SAE, the SSAAE shows more sensitivities to coating morphology for larger wavelength. The SSAAE of equivalent core-shell Mie model significantly differs from that of coated BC aggregates, and shows even negative values for some large D_p/D_c, indicating the limitation of core-shell Mie model in approximating

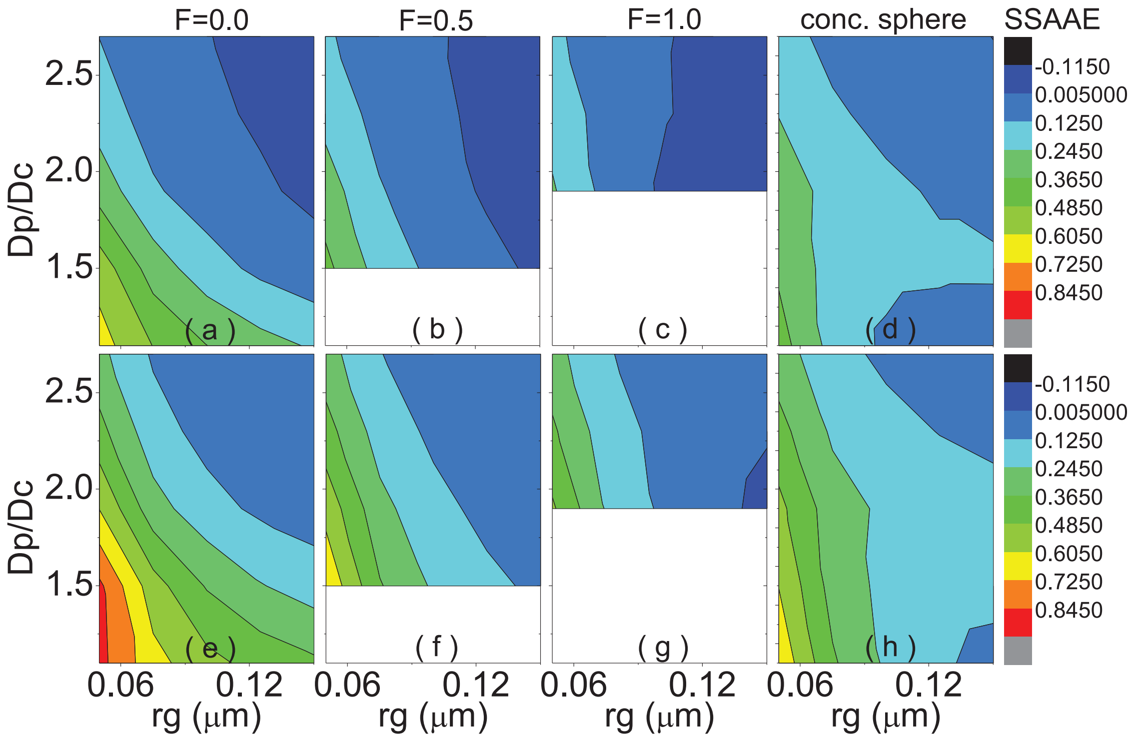

Fig. 6. Same as in Fig. 4 but for SSAAE.

the SSAAE of aged BC. The negative SSAAE may be a useful criterion for defining brown coating [19], as brown carbon exhibits an increase of its imaginary part of refractive index towards short wavelengths [e.g., 42].

Fig. 6 shows the impact of size distribution on the SSAAE of BC with non-absorbing coating. The SSAAE of coated BC aggregates is strongly dependent on size distribution, and it decreases with increasing r_g, which is similar to the pattern of the EAE. The $SSAAE_1$ and $SSAAE_2$ of coated BC aggregates alter from –0.03 to 0.66 and from 0.01 to 0.88 for externally attached BC-organics, respectively. Nevertheless, for fully coated BC aggregates, their $SSAAE_1$ and $SSAAE_2$ vary in ranges of –0.11–0.26 and –0.02–0.50, respectively. It is interesting to see that, BC coated by non-absorbing organics with large coated-BC size distribution can even show negative SSAAE values for some coating microphysics. Significant differences are found between the SSAAE values given by the core-shell Mie model and those of coated BC aggregates. In general, the shell/core ratio plays a more substantial role than other microphysical parameters of morphology in determining the EAE, AAE and SSAAE of coated BC aggregates with a fixed size distribution. Compared to shell/core ratio, the dependences of the EAE, AAE and SSAAE of coated BC aggregates on size distribution are higher, and the EAE and SSAAE are small for large coated BC size. Meanwhile, the EAE, AAE and SSAAE of coated BC aggregates show dependences on wavelength, and their values become high for large wavelength except for the AAE of externally attached BC-organics. The review by Kahnert and Kanngießer [29] also show that BC AAE and EAE depend on particle morphology, size, spectral range, BC volume fraction, and coating materials [32,37,43]. The Angstrom exponents of equivalent core-shell Mie model generally differ from those of coated BC aggregates significantly, and therefore, realistic aggregate structures may have to be employed for spectral varying optical properties of aged BC particles.

4. Conclusions

The study explores the influences of shell/core ratio, BC geometry, BC position inside coating, coated volume fraction of BC, and size distribution on the Angstrom exponents of coated BC aerosols. The fractal aggregate is used to model realistic BC geometry, while the MSTM is employed to calculate the Angstrom exponents of coated BC. The results indicate that coated volume fraction of BC has significant impacts on optical properties of coated BC, particularly the absorption. The impact of fractal dimension of BC on coated BC optical properties is negligible, in spite that it shows important influences on optical properties of bare BC aggregates. The EAE, AAE and SSAAE of coated BC aggregates with different particle size distributions vary in ranges of 0.3–1.5, 0.3–2.5 and –0.1–0.9, respectively. The shell/core ratio and size distribution play substantial roles in determining the EAE, AAE and SSAAE of coated BC, wherein the dependences of the Angstrom exponents on size distribution are higher. Meanwhile, the EAE, AAE and SSAAE of coated BC aggregates have dependences on incident wavelength, and their values generally become high for large wavelength. Our study also reveals that BC coated by non-absorbing organics with large coated-BC size distribution may show negative SSAAE values for some coating microphysics, and this implies the limitation of separating brown carbon from black carbon with a criterion of negative SSAAE. In addition, the core-shell Mie model may introduce significant errors if it is employed to approximate the Angstrom exponents of coated BC, and thus, accurate morphologies and models should be applied to account for rigorous spectral varying optical properties of aged BC aerosols. Moreover, besides the EAE, AAE and SSAAE investigated in our study, the backscattering Angstrom exponent (BAE) is another significant optical parameter, and the use of light polarization to investigate the size, shape, and refractive index dependence of BAE has been presented [44].

Author statement

M. Mao and X. Zhang conceived the research plan. X. Zhang performed the simulations and wrote the manuscript. All authors discussed the results and contributed the final paper.

Declaration of Competing Interest

The authors declare that they have no conflict of interest.

Acknowledgments

This work is financially supported by the National Natural Science Foundation of China (NSFC) (41505127), and Natural Science Foundation of Jiangsu Province (BK20150901). This work is also supported by the Key Laboratory of Middle Atmosphere and Global Environment Observation (LAGEO-2019–04), and Key Laboratory of Meteorological Disaster, Ministry of Education (KLME201810). We particularly acknowledge the source of the codes of MSTM 3.0 from Daniel W. Mackowski.

References

[1] Ramanathan V, Carmichael G. Global and regional climate changes due to black carbon. Nat Geosci 2008;1(4):221–7.
[2] Scarnato BV, Vahidinia S, Richard DT, Kirchstetter TW. Effects of internal mixing and aggregate morphology on optical properties of black carbon using a discrete dipole approximation model. Atmos Chem Phys 2013;13(10):5089–101.
[3] Bond TC, Doherty SJ, Fahey DW, Forster PM, Berntsen T, DeAngelo BJ, Flanner MG, Ghan S, Kaercher B, Koch D, Kinne S, Kondo Y, Quinn PK, Sarofim MC, Schultz MG, Schulz M, Venkataraman C, Zhang H, Zhang S, Bellouin N, Guttikunda SK, Hopke PK, Jacobson MZ, Kaiser JW, Klimont Z, Lohmann U, Schwarz JP, Shindell D, Storelvmo T, Warren SG, Zender CS. Bounding the role of black carbon in the climate system: a scientific assessment. J Geophys Res 2013;118(11):5380–552.
[4] Smith AJA, Peters DM, McPheat R, Lukanihins S, Grainger RG. Measuring black carbon spectral extinction in the visible and infrared. J Geophys Res 2015;120:9670–83.
[5] Pandey A, Chakrabarty RK, Liu L, Mishchenko MI. Empirical relationships between optical properties and equivalent diameters of fractal soot aggregates at 550 nm wavelength. Opt Express 2015;23(24):A1354–62.
[6] Zhang X, Mao M. Radiative properties of coated black carbon aerosols impacted by their microphysics. J Quant Spectrosc Radiat Transfer 2020;241:106718.
[7] China S, Mazzoleni C, Gorkowski K, Aiken AC, Dubey M. K. Morphology and mixing state of individual freshly emitted wildfire carbonaceous particles. Nat Commun 2013;4:2122.
[8] China S, Scarnato B, Owen RC, Zhang B, Ampadu MT, Kumar S, Dzepina K, Dziobak MP, Fialho P, Perlinger JA, Hueber J, Helmig D, Mazzoleni LR, Mazzoleni C. Morphology and mixing state of aged soot particles at a remote marine free troposphere site: implications for optical properties. Geophys Res Lett 2015;42:1243–50.
[9] Liu D, Taylor JW, Young DE, Flynn MJ, Coe H, Allan JD. The effect of complex black carbon microphysics on the determination of the optical properties of brown carbon. Geophys Res Lett 2015;42:613–19.
[10] Zhang Y, Zhang Q, Cheng Y, Su H, Kecorius S, Wang Z, Wu Z, Hu M, Zhu T, Wiedensohler A, He K. Measuring the morphology and density of internally mixed black carbon with SP2 and VTDMA: new insight into the absorption enhancement of black carbon in the atmosphere. Atmos Meas Tech 2016;9:1833–43.
[11] Liu L, Mishchenko MI. Scattering and radiative properties of complex soot and soot-containing aggregate particles. J Quant Spectrosc Radiat Transfer 2007;106(1):262–73.
[12] Bescond A, Yon J, Ouf FX, Ferry D, Delhaye D, Gaffie D, Roze C. Automated determination of aggregate primary particle size distribution by TEM image analysis: application to soot. Aerosol Sci Technol 2014;48(8):831–41.
[13] Dong J, Zhao JM, Liu LH. Morphological effects on the radiative properties of soot aerosols in different internally mixing states with sulfate. J Quant Spectrosc Radiat Transfer 2015;165:43–55.
[14] Moosmuller H, Chakrabarty RK. Technical Note: simple analytical relationships between Angstrom coefficients of aerosol extinction, scattering, absorption, and single scattering albedo. Atmos Chem Phys 2011;11:10677–80.
[15] Kaskaoutis DG, Kambezidis HD. Comparison of the Angstrom parameters retrieval in different spectral ranges with the use of different techniques. Meteorol Atmos Phys 2008;99:233–46.
[16] Costabile F, Barnaba F, Angelini F, Gobbi GP. Identification of key aerosol populations through their size and composition resolved spectral scattering and absorption. Atmos Chem Phys 2013;13:2455–70.
[17] Russell PB, Bergstrom RW, Shinozuka Y, Clarke AD, DeCarlo PF, Jimenez JL, Livingston JM, Redemann J, Dubovik O, Strawa A. Absorption AngstromExponent in AERONET and related data as an indicator of aerosol composition. Atmos Chem Phys 2010;10:1155–69.
[18] Lack DA, Cappa CD. Impact of brown and clear carbon on light absorption enhancement, single scatter albedo and absorption wavelength dependence of black carbon. Atmos Chem Phys 2010;10:4207–20.
[19] Chakrabarty RK, Moosmuller H, Chen LWA, Lewis K, Arnott WP, Mazzoleni C, Dubey MK, Wold CE, Hao WM, Kreidenweis SM. Brown carbon in tar balls from smoldering biomass combustion. Atmos Chem Phys 2010;10(13):6363–70.
[20] Chung CE, Lee K, Muller D. Effect of internal mixture on black carbon radiative forcing. Tellus B 2011;64(1):1–13.
[21] Li J, Liu C, Yin Y, Kumar KR. Numerical investigation on the Angstrom exponent of black carbon aerosol. J Geophys Res 2016;121:3506–18.
[22] Sorensen CM. Light scattering by fractal aggregates: a review. Aerosol Sci Technol 2001;35(2):648–87.
[23] Schwarz JP, Gao RS, Spackman JR, Watts LA, Thomson DS, Fahey DW, Ryerson TB, Peisch J, Holloway JS, Trainer M, Frost GJ, Baynard T, Lack DA, de Gouw JA, Warneke C, Del Negro LA. Measurement of the mixing state, mass, and optical size of individual black carbon particles in urban and biomass burning emissions. Geophys Res Lett 2008;35(13):L13810.
[24] Liu L, Mishchenko MI, Arnott WP. A study of radiative properties of fractal soot aggregates using the superposition T-matrix method. J Quant Spectrosc Radiat Transfer 2008;109(15):2656–63.
[25] Coz E, Leck C. Morphology and state of mixture of atmospheric soot aggregates during the winter season over Southern Asia–a quantitative approach. Tellus B 2011;63:107–16.
[26] Zhang X, Mao M, Yin Y, Wang B. Numerical investigation on absorption enhancement of black carbon aerosols partially coated with nonabsorbing organics. J Geophys Res 2018;123:1297–308.
[27] Zhang X, Mao M, Yin Y, Tang S. The absorption Angstrom exponent of black carbon with brown coatings: effects of aerosol microphysics and parameterization. Atmos. Chem. Phys. 2020;20:9701–11.
[28] Skorupski K, Mroczka J, Wriedt T, Riefler N. A fast and accurate implementation of tunable algorithms used for generation of fractal-like aggregate models. Physica A 2014;404:106–17.
[29] Kahnert M, Kanngießer F. Modelling optical properties of atmospheric black carbon aerosols. J Quant Spectrosc Radiat Transfer 2020;244:106849.
[30] Mackowski DW. A general superposition solution for electromagnetic scattering by multiple spherical domains of optically active media. J Quant Spectrosc Radiat Transfer 2014;133:264–70.
[31] Zhang X, Mao M, Chen H. Characterization of optically effective complex refractive index of black carbon composite aerosols. J Atmos Sol-Terr Phys 2020;198:105180.
[32] Zhang K, O'Donnell D, Kazil J, Stier P, Kinne S, Lohmann U, Ferrachat S, Croft B, Quaas J, Wan H, Rast S, Feichter J. The global aerosol-climate model ECHAM-HAM, version 2: sensitivity to improvements in process representations. Atmos Chem Phys 2012;12:8911–49.
[33] Luo J, Zhang Y, Wang F, Zhang Q. Effects of brown coatings on the absorption enhancement of black carbon: a numerical investigation. Atmos Chem Phys 2018;18(23):16897–914.
[34] Bond TC, Bergstrom RW. Light absorption by carbonaceous particles: an investigative review. Aerosol Sci Technol 2006;40:27–67.
[35] Kim H, Paulson SE. Real refractive indices and volatility of secondary organic aerosol generated from photooxidation and ozonolysis of limonene, alpha-pinene and toluene. Atmos Chem Phys 2013;13:7711–23.
[36] Zhang X, Mao M, Yin Y, Wang B. Absorption enhancement of aged black carbon aerosols affected by their microphysics: a numerical investigation. J Quant Spectrosc Radiat Transfer 2017;202:90–7.
[37] Cappa CD, Onasch TB, Massoli P, Worsnop DR, Bates TS, Cross ES, Davidovits P, Hakala J, Hayden KL, Jobson BT, Kolesar KR, Lack DA, Lerner BM, Li SM, Mellon D, Nuaaman I, Olfert JS, Petaja T, Quinn PK, Song C, Subramanian R, Williams EJ, Zaveri RA. Radiative absorption enhancements due to the mixing state of atmospheric black Carbon. Science 2012;337:1078–81.
[38] Schuster GL, Dubovik O, Holben BN. Angstrom exponent and bimodal aerosol size distributions. J Geophys Res 2006;111:D07207.
[39] Toledano C, Cachorro VE, Berjon A, De Frutos AM, Sorribas M, De la Morena BA, Goloub P. Aerosol optical depth and Ångström exponent climatology at El Arenosillo AERONET site (Huelva, Spain). Q J Roy Meteorol Soc 2007;133(624):795–807.
[40] Liu L, Mishchenko M. Scattering and radiative properties of morphologically complex carbonaceous aerosols: a systematic modeling study. Remote Sens 2018;10:1634.
[41] Liu C, Chung CE, Yin Y, Schnaiter M. The absorption Angstrom exponent of black carbon: from numerical aspects. Atmos Chem Phys 2018;18:6259–73.
[42] Moosmuller H, Chakrabarty RK, Arnott WP. Aerosol light absorption and its measurement: a review. J Quant Spectrosc Radiat Transfer 2009;110:844–78.
[43] Kahnert M, Nousiainen T, Lindqvist H. Models for integrated and differential scattering optical properties of encapsulated light absorbing carbon aggregates. Opt Express 2013;21:7974–92.
[44] Miffre A, Cholleton D, Rairoux P. On the use of light polarization to investigate the size, shape, and refractive index dependence of backscattering Angstrom exponents. Opt Lett 2020;45(5):1084–7.